PLOS ONE

RESEARCH ARTICLE

Combination therapy for cancer with oncolytic virus and checkpoint inhibitor: A mathematical model

Avner Friedman[1], **Xiulan Lai**[2]*

1 Mathematical Bioscience Institute & Department of Mathematics, Ohio State University, Columbus, OH, United States of America, **2** Institute for Mathematical Sciences, Renmin University of China, Beijing, P. R. China

* xiulanlai@ruc.edu.cn

OPEN ACCESS

Citation: Friedman A, Lai X (2018) Combination therapy for cancer with oncolytic virus and checkpoint inhibitor: A mathematical model. PLoS ONE 13(2): e0192449. https://doi.org/10.1371/journal.pone.0192449

Editor: Francesco Bertolini, European Institute of Oncology, ITALY

Received: August 6, 2017

Accepted: January 23, 2018

Published: February 8, 2018

Data Availability Statement: All relevant data are within the paper.

Funding: This work is supported by the Mathematical Biosciences Institute and the National Science Foundation (Grant DMS 0931642 to AF), and by the Renmin University of China and the International Postdoctoral Exchange Fellowship Program 2016 by the Office of China Postdoctoral Council. The funders had no role in study design, data collection and analysis, decision to publish, or preparation of the manuscript.

Abstract

Oncolytic virus (OV) is a replication competent virus that selectively invades cancer cells; as these cells die under the viral burden, the released virus particles proceed to infect other cancer cells. Oncolytic viruses are designed to also be able to stimulate the anticancer immune response. Thus, one may represent an OV by two parameters: its replication potential and its immunogenicity. In this paper we consider a combination therapy with OV and a checkpoint inhibitor, anti-PD-1. We evaluate the efficacy of the combination therapy in terms of the tumor volume at some later time, for example, 6 months from initial treatment. Since T cells kill not only virus-free cancer cells but also virus-infected cancer cells, the following question arises: Does increasing the amount of the checkpoint inhibitor always improve the efficacy? We address this question, by a mathematical model consisting of a system of partial differential equations. We use the model to construct, by simulations, an efficacy map in terms of the doses of the checkpoint inhibitor and the OV injection. We show that there are regions in the map where an increase in the checkpoint inhibitor actually decreases the efficacy of the treatment. We also construct efficacy maps with checkpoint inhibitor vs. the replication potential of the virus that show the same antagonism, namely, an increase in the checkpoint inhibitor may actually decrease the efficacy. These results have implications for clinical trials.

Introduction

PD-1 is an immunoinhibitory receptor predominantly expressed on activated T cells [1, 2]. Its ligand PD-L1 is upregulated on the same activated T cells, and in some human cancer cells [2, 3]. The complex PD-1-PD-L1 is known to inhibit T cell function [1]. Immune checkpoints are regulatory pathways in the immune system that inhibit its active response against specific targets. In the case of cancer, the complex PD-1-PD-L1 functions as an immune checkpoint for anti-tumor T cells. CTLA-4 is another immunoinhibitory receptor expressed on activated T cells; when it combines with its ligand B7 on dendritic cells, the complex CTLA-4-B7 acts as a

Competing interests: The authors have declared that no competing interest exist.

checkpoint inhibitor for anti-tumor T cells [4, 5]. There has been much progress in recent years in developing checkpoint inhibitors, primarily anti-PD-1 and anti-PD-L1 [6], and anti-CTLA-4 [7, 8].

Oncolytic virus (OV) is a genetically engineered virus that can selectively invade into and replicate within cancer cells while not harming normal healthy cells. OV therapy has been explored as an approach to combat cancer, and clinical trials were carried out on different types of cancer [9–12]. However, therapeutic efficacy remains a challenge [13, 14]. One of the factors that limits OV therapy is the antigenicity of the infected cells; the macrophages of the innate immune system recognize these cells and destroy them together with the virus particles inside them. For this reason, experimental studies considered combination of OV therapy with immune suppressive drugs [15–18].

In another direction, some studies consider OV with viruses designed to both replicate within cancer cells and stimulate cytotoxic T cells; such viruses include vesicular stomatitis virus [19, 20], Newcastle Disease Virus [21], vaccinia [22, 23], measle virus [24], and others [25, 26]. Advances in the design of various oncolytic viruses are reported in [27, 28]. The underlying assumption in these studies is that the virus will survive long enough, under the pressure of the innate immune attack, to activate a sufficiently large number of cytotoxic T cells that will eradicate or significantly reduce the cancer. To make this approach more effective, it was suggested to combine the OV drug with checkpoint inhibitors. Several mouse experiments, with different types of cancer cells, reported that both CTLA-4 and PD-L1 checkpoints blockade enhanced the OV therapy [29–33]. There are also several clinical trials with OV and checkpoint inhibitors [34–37].

In previous work the authors considered combination therapies with checkpoint inhibitor and, as a second agent, tumor vaccine [38] or BRAF inhibitor [39]. In the present paper the second agent is oncolytic virus. This poses a dilemma, since T cells kill not only virus-free cancer cells but also virus-infected cancer cells (thus reducing the anti-cancer effect of the virus), while checkpoint inhibitors enhance the T cells activities. Thus, it is natural to ask whether increasing the amount of the checkpoint inhibitor does always result in a decrease in tumor volume. We develop a mathematical model to address this question. We denote by γ_V the dose amount of the injected OV and by γ_A the dose amount of the checkpoint inhibitor, and define the efficacy of the treatment by (γ_V, γ_A) in terms of the tumor volume at some arbitrary time, for example, 24 weeks from the beginning of the treatment. We use the mathematical model to develop an efficacy map, and we find that there are regions in (γ_V, γ_A) plane where an increase in γ_A results in actual decrease in the efficacy. We denote by λ_{V_i} the replication rate of viruses within infected cancer cells. We then construct efficacy maps for $(\lambda_{V_i}, \gamma_A)$ and find regions where an increase in γ_A again results in decreased efficacy. In such regions, the indiscriminent killing of infected and uninfected cancer cells has pro-cancer effect. These have implications for clinical trials.

The mathematical model includes $CD4^+$ Th1 cells and $CD8^+$ T cells, macrophages, and dendritic cells. Dendritic cells are activated indirectly by the virus and by necrotic cancer cells, while macrophages are activated by virus-infected cancer cells. Macrophages engulf and destroy infected cancer cells, but they also kill, at a lesser rate, uninfected cancer cells. When a cancer cell is infected by an extracellular virus, the extracellular virus becomes an intracellular virus within the infected cell. Intracellular viruses multiply within the cancer cells and cause them to lyse, thereby releasing all their viruses to the extracellular environment. T cells are activated by IL-12 produced by dendritic cells, and they also proliferate by IL-2 produced by Th1 cells. Fig 1 shows the network of interactions among the cells, with PD-1 and PD-L1 on T cells and PD-L1 also on tumor cells.

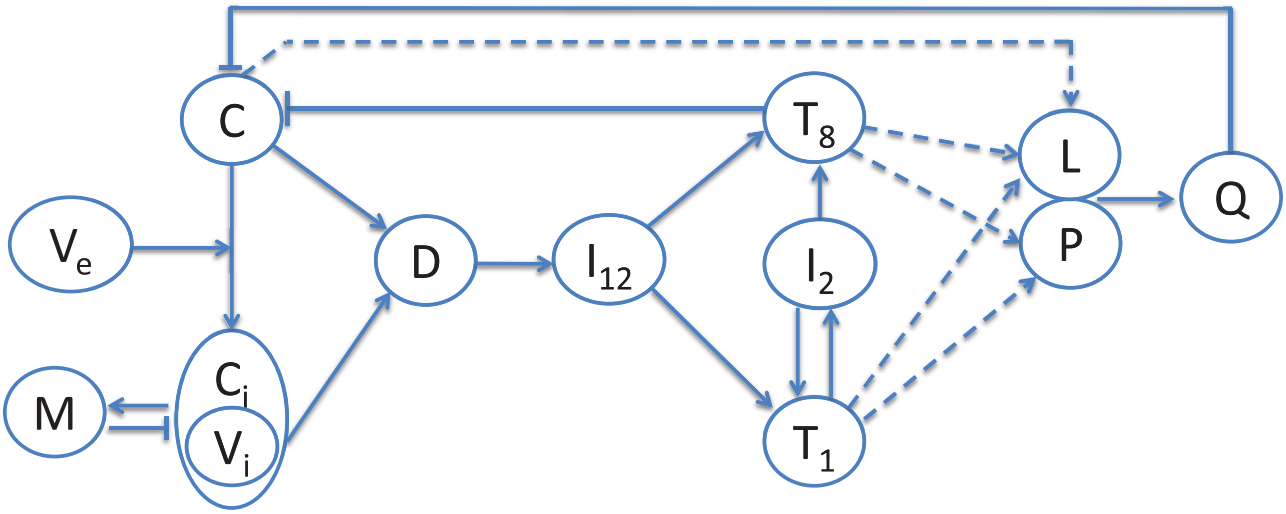

Fig 1. Interaction of tumor cells with virus and immune cells. Sharp arrows indicate proliferation/activation, blocked arrows indicate killing/blocking, and dashed lines indicate proteins on T cells. C: uninfected cancer cells, C_i: infected cancer cells, V_e: extracellular virus, V_i: intracellular virus, D: dendritic cells, T_1: $CD4^+$ Th1 cells, T_8: $CD8^+$ T cells, I_2: IL-2, I_{12}: IL-12, P: PD-1, L: PD-L1, Q: PD-1-PD-L1 complex.

https://doi.org/10.1371/journal.pone.0192449.g001

We assume that the treatment with combination therapy extends over a period of 16 weeks, and we evaluate the results of the treatment at the end of 24 weeks. We can use the model to compute the tumor volume at the end of 24 weeks for each pair of parameters of $(\lambda_{V_i}, \lambda_{DV})$ and doses (γ_A, γ_V).

The mathematical model is represented by a system of partial differential equations based on Fig 1.

Mathematical model

The mathematical model is based on the diagram in Fig 1. The list of variables is given in Table 1, where the density of cells and concentration of cytokines are all in unit of g/cm^3. The time unit is 1 day.

We assume that the total density of cells within the tumor remains constant in space and time, so that

$$C + C_i + M + D + T_1 + T_8 = \text{constant} = \theta. \quad (1)$$

Since cancer cells proliferate while T cells and macrophages enter the tumor, the assumption (1) implies that there is an internal pressure among cells, and this gives rise to a velocity **u** of cells.

Table 1. List of variables (in units of g/cm^3).

Notation	Description	Notation	Description
C	density of cancer cells	T_8	density of activated $CD8^+$ T cells
C_i	density of infected cancer cells	I_{12}	IL-12 concentration
V	density of extracellular virus	I_2	IL-2 concentration
V_i	density of intracellular virus	P	PD-1 concentration
M	density of macrophages	L	PD-L1 concentration
D	density of dentritic cells	Q	PD-1-PD-L1 concentration
T_1	density of activated $CD4^+$ T cells	A	anti-PD-L1 concentration

https://doi.org/10.1371/journal.pone.0192449.t001

Equation for uninfected cancer cells (C). We assume a logistic growth for cancer cells, and that cancer cells are killed primarily by $CD8^+$ T cells at a rate $\eta_8 T_8 C$ where η_8 is a constant. Cancer cells become infected by V_e at a rate proportional to CV_e. Therefore C satisfies the following equation:

$$\frac{\partial C}{\partial t} + \nabla \cdot (\mathbf{u}C) - \delta_C \nabla^2 C = \underbrace{\lambda_C C\left(1 - \frac{C}{C_M}\right)}_{\text{growth}} - \underbrace{\beta_C C V_e}_{\text{infection by } V_e} - \underbrace{\eta_8 T_8 C}_{\text{killed by CD8}^+ \text{ T cells}} - \underbrace{d_C C}_{\text{death}}, \tag{2}$$

where δ_C is the dispersion coefficient and d_C is the death rate by apoptosis.

Equation for infected cancer cells (C_i). We assume that $CD8^+$ T cells kill infected cancer cells at a rate $\eta_{8C_i} T_8 C_i$, where η_{8C_i} is a constant larger than η_8. We also assume that macrophages kill infected cancer cells by phagocytosis [40] at a rate proportional to $C_i M$. The death rate of infected cancer cells is larger than the death rate of uninfected cancer cells by a factor $\mu_{V_i} V_i$ which represents the effect of viral burden. We take the rate by which cancer cells become infected to be $\beta_C CV_e$. We finally assume that the density of the V_i cells is proportional to the density of the C_i cells within which the V_i reside, so that they have the same dispersion coefficient. Hence the equation for infected cancer cells is given by

$$\frac{\partial C_i}{\partial t} + \nabla \cdot (\mathbf{u}C_i) - \delta_{C_i} \nabla^2 C_i = \beta_C C V_e - \underbrace{d_C(1 + \mu_{V_i} V_i) C_i}_{\text{death}} - \underbrace{\mu_{C_i M} C_i M}_{\text{killed by } M} - \underbrace{\eta_{8C_i} T_8 C_i}_{\text{killed by CD8}^+ \text{ T cells}}. \tag{3}$$

Equation for extracellular virus (V_e). We assume that virus at amount γ_V is injected into the tumor at successive days $t_1, t_2, \ldots, t_n$. Thus at each day t_j we have to increase V_e by an amount γ_V, that is, $V_e(t_j + 0) - V_e(t_j - 0) = \gamma_V$. This increase can be written in the form

$$\left.\frac{dV_e}{dt}\right|_{t=t_j} = \gamma_V \delta(t - t_j)$$

where $\delta(s)$ is the Dirac measure. We assume that when an infected cell dies the intracellular viral particles are released into the tumor microenvironment; however, when an infected cell is killed by macrophages or T_8 cells, the virus particles inside it are cleared out. Extracellular virus are endocytosed by macrophages, and the rate of their depletion is proportional to MV_e. Hence, the equation for V_e takes the following form:

$$\frac{\partial V_e}{\partial t} - \delta_{V_e} \nabla^2 V_e = \sum_{j=1}^{m} \gamma_V \delta(t - t_j) + \underbrace{N d_C (1 + \mu_{V_i} V_i) V_i}_{\text{released by } C_i \text{ death}} - \underbrace{\beta_V C V_e}_{V_e \to V_i} - \underbrace{\mu_{V_e M} M V_e}_{\text{endocytosed by } M}, \tag{4}$$

where N is the average number of viral particles released at death of an infected cancer cell. Note that the coefficient β_V is related to the coefficient β_C in Eq (2) by the equation $\beta_V = \beta_C m_{VC}$, where m_{VC} is the ratio of the mass of one virus to one cancer cell.

Equation for intercellular virus (V_i). Viruses multiply in a cancer cell by exploiting the DNA of the cell as a 'resource'. We represent the proliferation of the viruses in the cell by $\lambda_{V_i} C_i$. The equation for V_i is the following:

$$\frac{\partial V_i}{\partial t} + \nabla \cdot (\mathbf{u} V_i) - \delta_{C_i} \nabla^2 V_i = \underbrace{\beta_V C V_e}_{V_e \to V_i} + \underbrace{\lambda_{V_i} C_i}_{\text{growth of } V_i \text{ in } C_i} - \underbrace{N d_C (1 + \mu_{V_i} V_i) V_i}_{\text{released through death of } C_i} - \underbrace{\mu_{C_i M} V_i M}_{\text{killed by } M} - \underbrace{\eta_{8C_i} T_8 V_i}_{\text{killed by CD8}^+ \text{cells}} . \tag{5}$$

The last two terms represent a loss of V_i due to death of their host C_i by the macrophages and $CD8^+$ T cells. Note that V_i moves with the same velocity $\vec{u}$ as C_i.

Equation for macrophages (M). The growth rate of the proinflammatory macrophages is promoted by infected cancer cells and is represented by a term $\lambda_{MC_i} M C_i$. Hence M satisfies the following equation:

$$\frac{\partial M}{\partial t} + \nabla \cdot (\mathbf{u} M) - \delta_M \nabla^2 M = \underbrace{\lambda_M}_{\text{Source}} + \underbrace{\lambda_{MC_i} M C_i}_{\text{growth}} - \underbrace{d_M M}_{\text{death}}, \tag{6}$$

where λ_M is a source of macrophages prior to the treatment with OV.

Equation for dentritic cells (D). Oncolytic virus is often armed to elicit adaptive immune response [19, 24]. In particular, we assume that inactive dendritic cells with density D_0 are activated by intracellular armed viruses at a rate proportional to $D_0 V_i$. Dendritic cells are also activated by HMGB-1 [41, 42], which is produced by necrotic cancer cells (NCs) [43]. We assume that the concentration of HMGB-1 is proportional to the density of NCs and that the density of NCs is proportional to the density of cancer cells. Hence, the activation rate of inactive dendritic cells is proportional to $D_0 \frac{C}{K_C + C}$, where the Michaelis-Menten law is used to account for the limited receptor recycling time which occurs in the process of DC activation. The dynamics of DCs is given by

$$\frac{\partial D}{\partial t} + \underbrace{\nabla \cdot (\mathbf{u} D)}_{\text{velocity}} - \underbrace{\delta_D \nabla^2 D}_{\text{difusion}} = \underbrace{\lambda_{DV} D_0 V_i}_{\text{activation by intracellular virus}} + \underbrace{\lambda_{DC} D_0 \frac{C}{K_C + C}}_{\text{activation by HMGB}-1} - \underbrace{d_D D}_{\text{death}}, \tag{7}$$

Equation for $CD4^+$ T cells (T_1). Naive $CD4^+$ T cells are activated by IL-12 while in direct contact with dendritic cells. IL-2 induces proliferation of activated T_1 cells [44, 45]. Both processes are inhibited by the complex PD-1-PD-L1 (Q) [46], by a factor $\frac{1}{1+Q/K_{TQ}}$. Hence T_1 satisfies

the following equation:

$$\frac{\partial T_1}{\partial t} + \nabla \cdot (\mathbf{u} T_1) - \delta_T \nabla^2 T_1 = \underbrace{\left(\hat{\lambda}_{T_1 I_{12}} T_{10} \frac{I_{12}}{K_{I_{12}} + I_{12}} \frac{D}{K_D + D} \right)}_{\text{activation by IL-12}} + \underbrace{\lambda_{T_1 I_2} T_1 \frac{I_2}{K_{I_2} + I_2}}_{\text{promotion by IL-2}} \times \underbrace{\frac{1}{1 + Q/K_{TQ}}}_{\text{inhibition by PD-1-PD-L1}} - \underbrace{d_{T_1} T_1}_{\text{death}} . \tag{8}$$

Equation for CD8$^+$ T cells (T_8). IL-12 activates CD8$^+$ T cells and IL-2 induces proliferation of CD8$^+$ T cells [44, 45]. Hence, similarly to the equation for T_1, T_8 satisfies the following equation:

$$\frac{\partial T_8}{\partial t} + \nabla \cdot (\mathbf{u} T_8) - \delta_T \nabla^2 T_8 = \underbrace{\left(\hat{\lambda}_{T_8 I_{12}} T_{80} \frac{I_{12}}{K_{I_{12}} + I_{12}} \frac{D}{K_D + D} \right)}_{\text{activation by IL-12}} + \underbrace{\lambda_{T_8 I_2} T_1 \frac{I_2}{K_{I_2} + I_2}}_{\text{promotion by IL-2}} \times \underbrace{\frac{1}{1 + Q/K_{TQ}}}_{\text{inhibition by PD-1-PD-L1}} - \underbrace{d_{T_8} T_8}_{\text{death}} . \tag{9}$$

Equation for IL-12 (I_{12}). IL-12 is produced by activated DCs, so that

$$\frac{\partial I_{12}}{\partial t} - \delta_{I_{12}} \nabla^2 I_{12} = \underbrace{\lambda_{I_{12} D} D}_{\text{production by DCs}} - \underbrace{d_{I_{12}} I_{12}}_{\text{degradation}} . \tag{10}$$

The diffusion coefficient of I_{12} is several orders of magnitude larger than the diffusion coefficient of cells. Hence the transport term $\nabla \cdot (\mathbf{u} I_{12})$ is negligible compared to the diffusion term $\delta_{I_{12}} \nabla^2 I_{12}$, and it was therefore omitted.

Equation for IL-2 (I_2). IL-2 is produced by activated CD4$^+$ T cells. Hence,

$$\frac{\partial I_2}{\partial t} - \delta_{I_2} \nabla^2 I_2 = \underbrace{\lambda_{I_2 T_1} T_1}_{\text{production by } T_1} - \underbrace{d_{I_2} I_2}_{\text{degradation}} . \tag{11}$$

Here again the transport term was omitted.

Equation for PD-1 (P), PD-L1 (L) and PD-1-PD-L1 (Q). PD-1 is expressed on the surface of activated CD4$^+$ T cells and activated CD8$^+$ T cells. Hence, P is given by $P = \rho_P(T_1 + T_8)$, where ρ_P is the ratio of the mass of all the PD-1 proteins in one T cell to the mass of one T cell. Thus, P satisfies the equation

$$\frac{\partial P}{\partial t} + \nabla \cdot (\mathbf{u} P) - \delta_T \nabla^2 P = \rho_P \left[\frac{\partial (T_1 + T_8)}{\partial t} + \nabla \cdot (\mathbf{u}(T_1 + T_8)) - \delta_T \nabla^2 (T_1 + T_8) \right],$$

or, by Eqs (8) and (9),

$$\frac{\partial P}{\partial t} + \nabla \cdot (\mathbf{u} P) - \delta_T \nabla^2 P = \rho_P \left[(\lambda_{T_1 I_{12}} T_{10} + \lambda_{T_8 I_{12}} T_{80}) \frac{I_{12}}{K_{I_{12}} + I_{12}} + (\lambda_{T_1 I_2} T_1 + \lambda_{T_8 I_2} T_8) \frac{I_2}{K_{I_2} + I_2} \right] \times \frac{1}{1 + Q/K_{TQ}} - \rho_P (d_{T_1} T_1 + d_{T_8} T_8),$$

where $\rho_P = \frac{P}{T_1+T_8}$. Note that P undergoes the same advection velocity $\vec{u}$ as the T cells. We assume that PD-1 is depleted (or blocked) by A at rate $\mu_{PA}PA$, so that

$$\frac{\partial P}{\partial t} + \nabla \cdot (\mathbf{u}P_1) - \delta_T \nabla^2 P = \frac{P}{T_1+T_8}\left[(\lambda_{T_1I_{12}}T_{10} + \lambda_{T_8I_{12}}T_{80})\frac{I_{12}}{K_{I_{12}}+I_{12}} + (\lambda_{T_1I_2}T_1 + \lambda_{T_8I_2}T_8)\frac{I_2}{K_{I_2}+I_2}\right] \times \frac{1}{1+Q/K_{TQ}} - \frac{P}{T_1+T_8}(d_{T_1}T_1 + d_{T_8}T_8) - \underbrace{\mu_{PA}PA}_{\text{depletion by anti-PD-1}}. \tag{12}$$

In the sequal we take the dimension of μ_{PA} to be $\text{cm}^3/\text{g} \cdot \text{day}$ so that A is given in unit of g/cm^3.

PD-L1 is expressed on the surface of activated $CD4^+$ T cells, activated $CD8^+$ T cells, and on tumor cells. Hence, the concentration of PD-L1 (L) is proportional to ($T_1 + T_8$) and C:

$$L = \rho_L(T_1 + T_8 + \varepsilon C), \tag{13}$$

where ρ_L is the ratio of the mass of all the PD-L1 proteins in one T cell to the mass of one T cell, and ε depends on the specific type of tumor.

PD-1 and PD-L1 form a complex PD-1-PD-L1 (Q), with association and disassociation rates α_{PL} and d_Q, respectively:

$$P + L \underset{d_Q}{\overset{\alpha_{PL}}{\rightleftharpoons}} Q. \tag{14}$$

The half-life of Q is less then 1 second (i.e. 1.16×10^{-5} day) [47]. Hence, we may assume that the dynamics in (14) is in quasi-steady state, so that $\alpha_{PL}\, PL = d_Q\, Q$, or

$$Q = \sigma PL, \tag{15}$$

where $\sigma = \alpha_{PL}/d_Q$.

Equation for anti-PD-1 (A). We assume that anti-PD-1 is injected intraperitoneally in the amount γ_A at the same days $t_1, t_2, ..., t_n$ as in the injection of virus. The PK/PD effect of the drug is assumed to be $\sum_{j=1}^{n} \gamma_A H(t-t_j)e^{-\alpha(t-t_j)}$, where $H(s) = 0$ if $s \leq 0$, $H(t) = 1$ if $s > 1$. The drug A is depleted in the process of blocking PD-1. Hence,

$$\frac{\partial A}{\partial t} - \delta_A \nabla^2 A = \underbrace{\sum_{j=1}^{n} \gamma_A H(t-t_j)e^{-\alpha(t-t_j)}}_{\text{injection}} - \underbrace{\mu_{AP}PA}_{\text{depletion through blocking PD-1}} - \underbrace{d_A A}_{\text{degradation}}. \tag{16}$$

Equation for cells velocity (u): Cells disperse within the tissue, and its random motility may vary from one cell type to another. If the differences in the dispersion coefficients are ignored, then by adding the equations for all the cells and using Eq (1), we get

$$\theta \times \nabla \cdot \mathbf{u} = \text{Right} - \text{hand side of Eqs (2), (3) and (6)-(9)}.$$

To simplify the model we assume that the differences between the dispersion coefficients of the different cell types are small (but see comments in "Parameter estimation" (in "Diffusion coefficients") and "Sensitivity analysis"), and proceed to use the above equation for $\nabla \cdot \mathbf{u}$.

We assume that the average density of each cell type eventually stabilizes with the following values: For cancer cells, 0.4 g/cm^3; for dendritic cells 0.4×10^{-4} g/cm^3; for macrophage, 0.2 g/cm^3; for T_1 cells, 2×10^{-3} g/cm^3; and for T_8 cells, 1×10^{-3} g/cm^3. Recalling Eq (1) we find that $\theta = 0.6034$, so that

$$0.6034 \times \nabla \cdot \mathbf{u} = \text{RHS of Eq (2)} + \text{RHS of Eq (3)} + \sum_{j=6}^{9} [\text{RHS of Eq (j)}]. \tag{17}$$

To simplify the computations, we assume that the tumor is spherical with moving boundary $r = R(t)$, and that all the densities and concentrations are radially symmetric, that is, functions of (r, t), where $0 \le r \le R(t)$. In particular, $\mathbf{u} = u(r, t)\mathbf{e}_r$, where $\mathbf{e}_r$ is the unit radial vector.

Equation for free boundary (*R*): We assume that the free boundary $r = R(t)$ moves with the velocity of cells, so that

$$\frac{dR(t)}{dt} = u(R(t), t). \tag{18}$$

Boundary conditions We assume that naive CD4$^+$ T cells and CD8$^+$ T cells which migrated from the lymph nodes into the tumor microenvironment have constant densities $\hat{T}_8$ at the tumor boundary, and that they are activated by dentritic cells and IL-12 upon entering the tumor. We represent this process by the flux conditions at the boundary:

$$\frac{\partial T_8}{\partial n} + \sigma_T(I_{12})(T_8 - \hat{T}_8) = 0, \quad \frac{\partial T_1}{\partial n} + \sigma_T(I_{12})(T_1 - \hat{T}_1) = 0 \quad \text{at } r = R(t), \tag{19}$$

where $\sigma_T(I_{12}) = \alpha_T \frac{I_{12}}{K_{I_{12}+I_{12}}} \frac{D}{K_D+D}$.

We impose zero-flux boundary condition on all the remaining variables:

$$\text{zero-flux for } C,\ C_i,\ V_e,\ V_i,\ M,\ D,\ I_{12},\ I_2,\ P,\ A(r,t) \quad \text{at } r = R(t). \tag{20}$$

It is implicity assumed that receptors P become expressed only after T_1 and T_8 cells were already inside the tumor.

Initial conditions We prescribe the following values (in unit g/cm^3) at day $t = 0$:

$$\begin{aligned} &R(0) = 0.01 \text{ cm, and } C = 0.3583, \\ &C_i = 0,\ V_e = 0,\ V_i = 0,\ T_1 = 3 \times 10^{-3},\ T_8 = 1.5 \times 10^{-3},\ M = 0.24, \\ &D = 6 \times 10^{-4}, I_2 = 3.5 \times 10^{-11}, I_{12} = 12 \times 10^{-10},\ P = 1.2 \times 10^{-9} \text{ g/cm}^3, \end{aligned} \tag{21}$$

Note that the initial values satisfy Eq (1). We took the initial values for cells to be different from their above assumed asymptotic values. The choice of the initial conditions have little effect on the simulation results after a few days.

Results

The simulations of the model were performed by Matlab based on the moving mesh method for solving partial differential equations with free boundary [48] (see the section on computational method).

Fig 2 shows the profiles of the average densities/concentrations of all the variables of the model in the first 30 days in the control case, that is, without treatment. The simulation results show that the steady states of all the cytokines and cells are approximately equal to the half-saturation values that we assumed in estimating the parameters of the model.

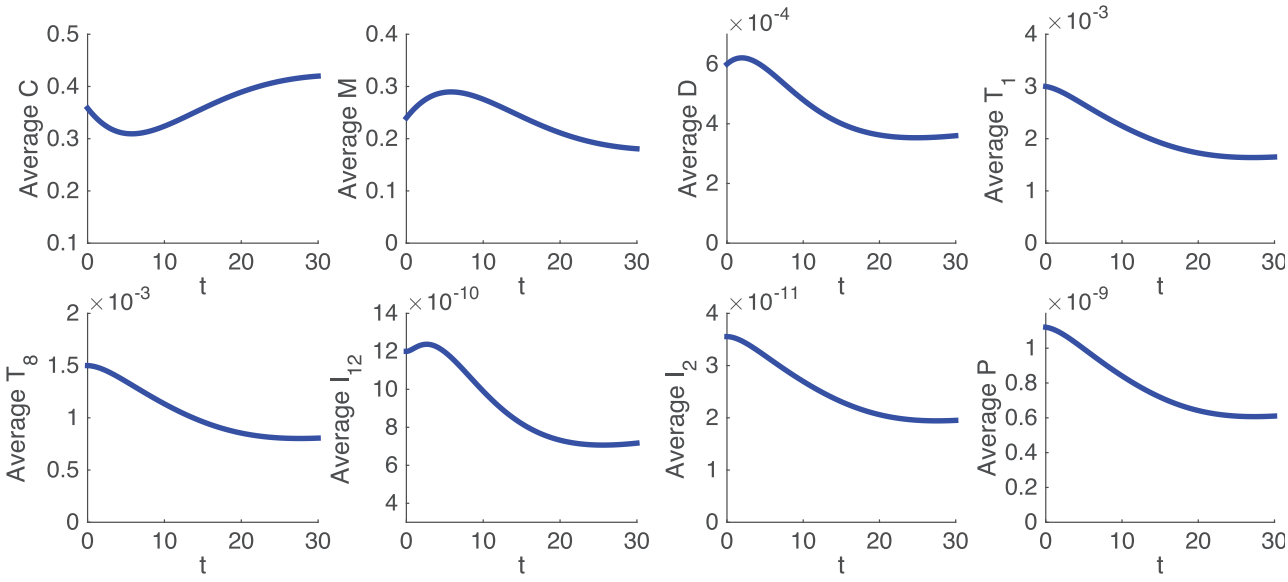

Fig 2. Average densities/concentrations, in g/cm^3, of all the variables in the model in the control case. All parameter values are the same as in Tables 2 and 3. Initial values are as in (21).

https://doi.org/10.1371/journal.pone.0192449.g002

We proceed to simulate the treatment of cancer by OV and anti-PD-1 as single agents, and by a combination of the two drugs. Following mice experiments reported in [49], we apply the OV injections in days 0,2,4, and anti-PD-1 injection in days 4,7,11. From Figs 1(b) and 2(b) in [49] we see that although all the mice were identical and were treated with the same amounts of dose, their responses were varied: For some mice the tumor volume grew faster with OV than with anti-PD-1 as single agents, while for others this was the reverse, which means that the "effective" dose amounts varied with each subject. We account for this, in our model, by taking for each mouse somewhat different values of γ_V and γ_A which represent the effective doses for this subject. We also note that γ_V and γ_A should be approximately proportional to the amount of dose injected in the experiments. We determined the proportionality coefficients, or rather the orders of the magnitude of γ_V and γ_A, so that the doubling time of the tumor volume (under treatment with a single agent) is approximately 20 days, which is the case for a large number of the mice in Figs 1(b), 2(b) of [49].

Fig 3(a)–3(c) show some simulations of the model with different values of γ_V and γ_A. The profiles are similar to many of those given in [49]. In Fig 3(a) treatment with anti-PD-1 as single agent reduces tumor growth more than treatment with OV as single agent, and in Fig 3(b) and 3(c), it is the reverse, in agreement with profiles in [49]. In all cases, the combination reduces the tumor growth more than a single agent.

We can characterize the anticancer effectiveness of a virus by (i) its ability to replicate within cancer cells, as represented by the parameters λ_{V_i} in Eq (5), and (ii) by its ability to stimulate the anticancer immune response, as represented by the activation rate λ_{DV} in Eq (7). For any pair $(\lambda_{V_i}, \lambda_{DV})$ we may associate a "virtual virus" having these two parameters.

We proceed to use the mathematical model to conduct *in silico* clinical trials. As an example, a treatment will be given for a period of 16 weeks, and the patient's tumor volume will be measured at the end of 24 weeks from the initial treatment. The virus is injected into the tumor at the beginning of weeks 1,3,5,7,9,11,13 and 15, at an amount γ_V, and the anti-PD-1 is given at the beginning of weeks 1,4,7,10, 13, 16 at an amount γ_A. We denote by $V_{24}(\gamma_V, \gamma_A)$ the

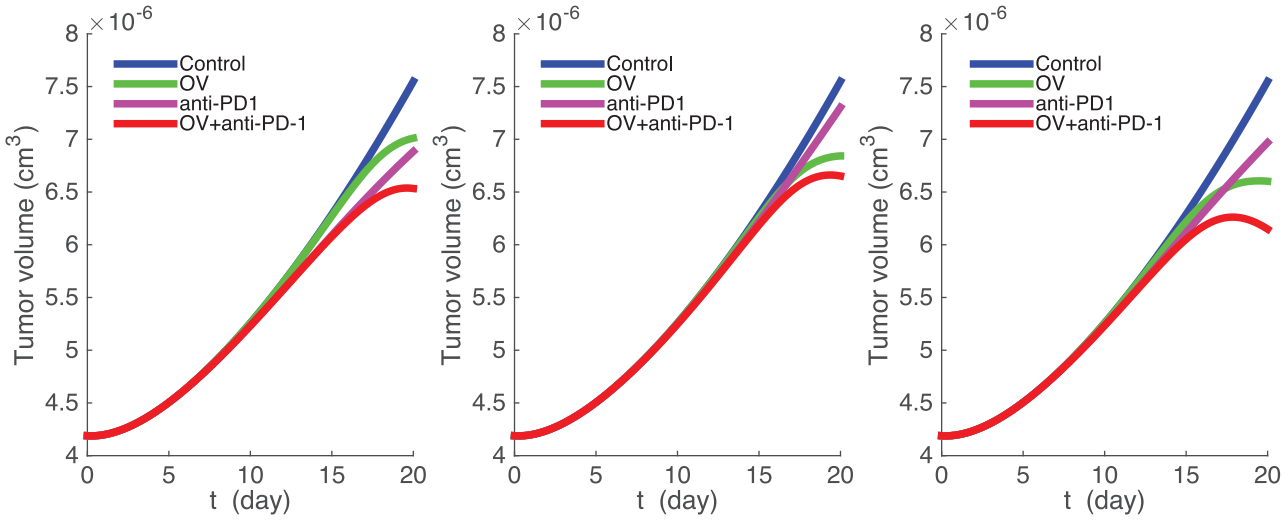

Fig 3. The growth of tumor volume. OV is given at days $t = 0, 2, 4$ with the amount γ_V and anti-PDE-1 is given at days $t = 4, 7, 11$ with the amount γ_A. (a) $\gamma_V = 0.1 \times 10^{-10}$ g/cm^3, $\gamma_A = 8 \times 10^{-7}$ g/cm^3. (b) $\gamma_V = 0.2 \times 10^{-10}$ g/cm^3, $\gamma_A = 3 \times 10^{-7}$ g/cm^3. (c) $\gamma_V = 0.5 \times 10^{-10}$ g/cm^3, $\gamma_A = 7 \times 10^{-7}$ g/cm^3. Parameter values are the same as in Fig 2.

https://doi.org/10.1371/journal.pone.0192449.g003

volume of the tumor at the end of 24 weeks, and define the efficacy of the treatment by the formula:

$$E(\gamma_V, \gamma_A) = \frac{V_{24}(0,0) - V_{24}(\gamma_V, \gamma_A)}{V_{24}(0,0)};$$

thus the efficacy is increased if the tumor volume $V_{24}(\gamma_V, \gamma_A)$ is decreased.

Fig 4 shows an efficacy map for the parameters $\lambda_{V_i} = 5 \times 10^{-4}$/day, $\lambda_{DV} = 5.2 \times 10^{10}$ cm^3/g · day. For clarity we marked tumor volumes $V_{24}(\gamma_V, \gamma_A)$ on the equi-efficacy curves. We see that as γ_V increases so does the efficacy. However, the same is not true of γ_A: there are regions where the efficacy decreases as γ_A increases. To understand what happens in such regions we take two points with the same γ_V: $(3.7 \times 10^{-7}, 5.4 \times 10^{-8})$ and $(3.7 \times 10^{-7}, 6.6 \times 10^{-8})$. Fig 5 shows that the tumor volume for the larger γ_A is somewhat larger than the tumor volume for the smaller γ_A. Fig 6 explains what has actually occurred. With the higher dose, more infected cancer cells were killed, and the virus population decreased. Hence the number of activated dendritic cells decreased and then also the number of T cells decreased, which resulted in an increase in the number of uninfected cancer cells.

We find the same phenomenon in Fig 7, which is an efficacy map for $(\gamma_A, \lambda_{V_i})$, for specific values of $\gamma_V = 2.5 \times 10^{-7}$ g/cm^3/day and $\lambda_{DV} = 5.2 \times 10^{10}$ cm^3/g · day. The tumor volume decreases as λ_{V_i} increases, but there are values of λ_{V_i} for which the tumor volume increases when γ_A is increased.

We note that λ_{DV} and γ_A are positively correlated, since both are increasing the activity of effector T cells. We therefore expect that, unlike situation in Fig 4, the tumor volume will decrease as γ_A increases.

One is tempted to replace PDE system by a simpler system of ODEs where the diffusion and advection terms are dropped. However, since the diffusion of cells is several orders of magnitude smaller than diffusion of cytokines and extracellular virus, the ODE system cannot

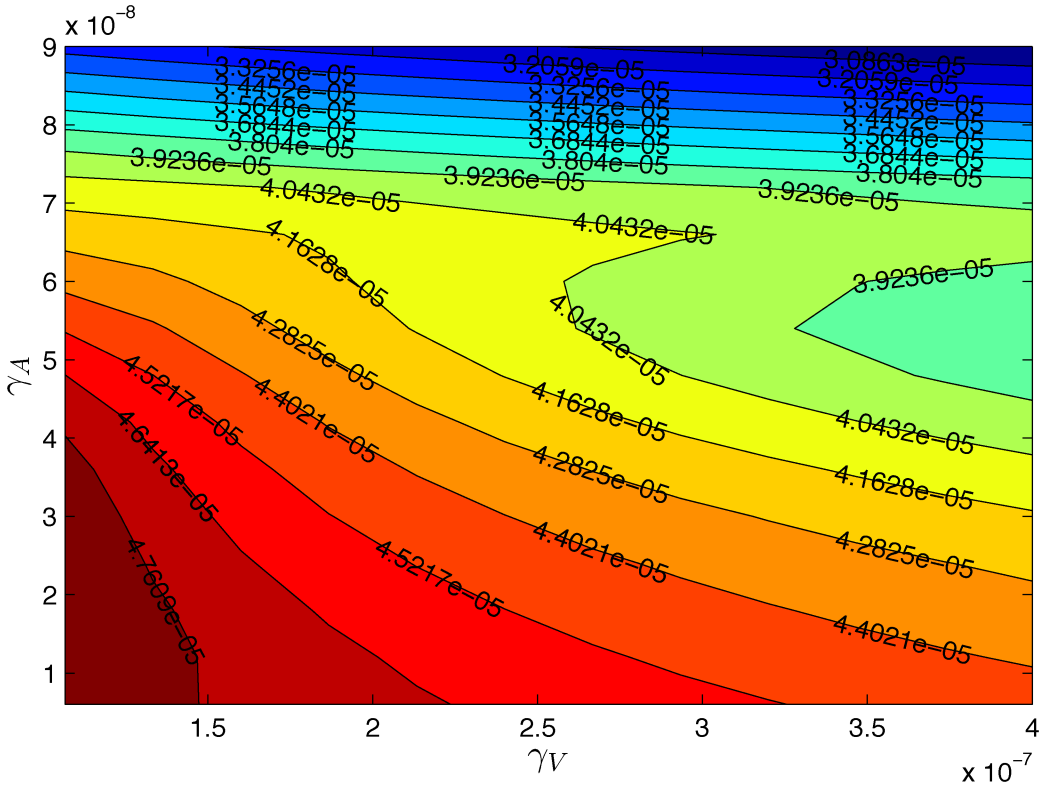

Fig 4. The tumor volume at week 24 for different pair of (γ_V, γ_A). Here $\lambda_{V_i} = 5 \times 10^{-4}$/day, $\lambda_{DV} = 5.2 \times 10^{10}$ cm^3/g · day, $\gamma_V = 1 \times 10^{-7} - 4 \times 10^{-7}$ g/cm^3 and $\gamma_A = 0.6 \times 10^{-8} - 9 \times 10^{-8}$ g/cm^3. All other parameter values are the same as in Tables 2 and 3.

https://doi.org/10.1371/journal.pone.0192449.g004

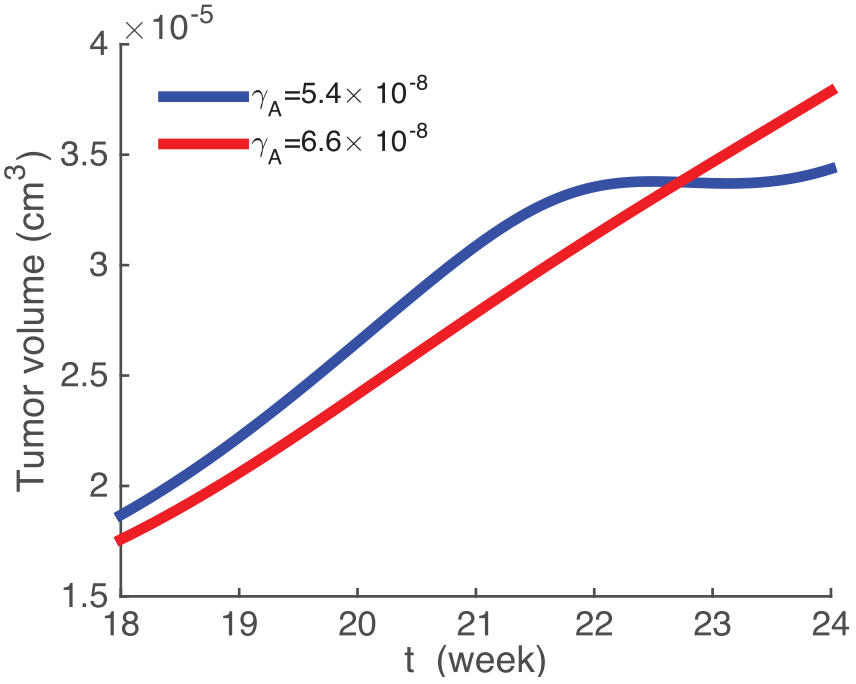

Fig 5. Growth of tumor volume. Here, $\gamma_V = 3.7 \times 10^{-7}$ g/cm^3. Other parameter values are the same as in Fig 4.

https://doi.org/10.1371/journal.pone.0192449.g005

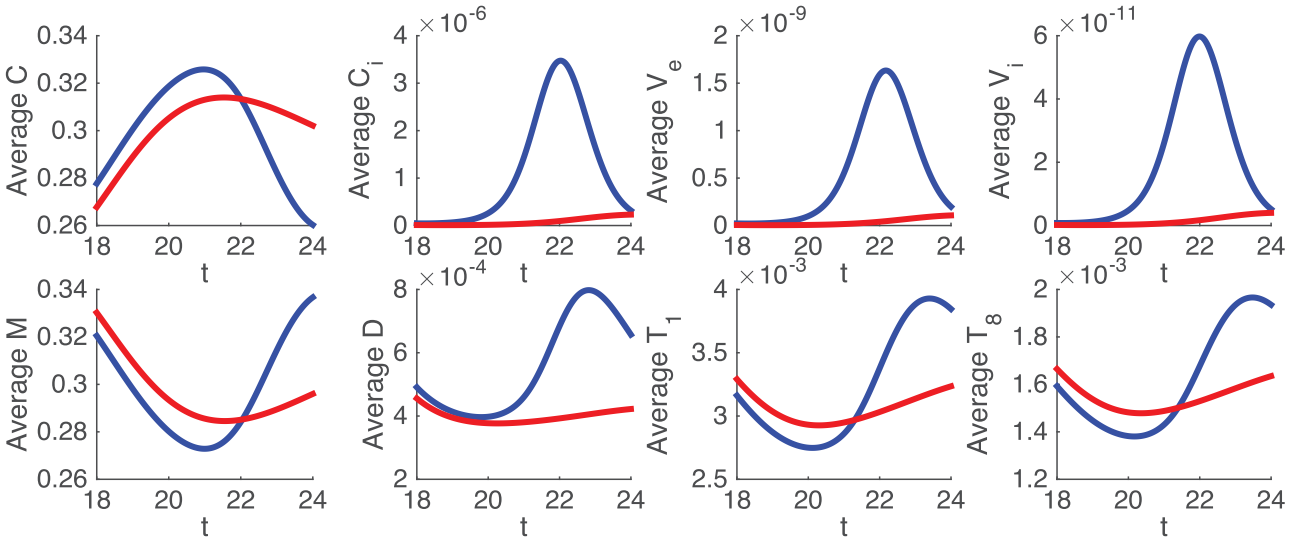

Fig 6. The average densities and tumor volume. Blue: $\gamma_V = 3.7 \times 10^{-7}$ g/cm^3, $\gamma_A = 5.4 \times 10^{-8}$ g/cm^3. Red: $\gamma_V = 3.7 \times 10^{-7}$ g/cm^3, $\gamma_A = 6.6 \times 10^{-8}$ g/cm^3. Other parameter values are the same as in Fig 4.

https://doi.org/10.1371/journal.pone.0192449.g006

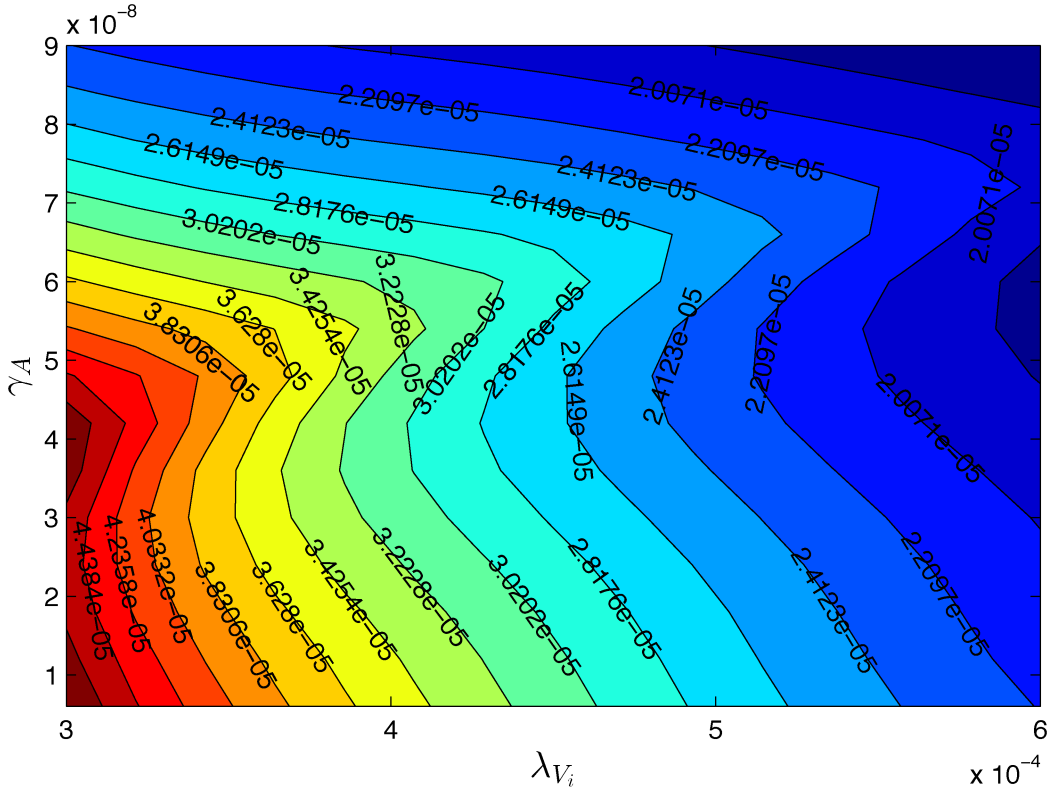

Fig 7. The tumor volume at week 24. Here, $\gamma_V = 2.5 \times 10^{-7}$ g/cm^3 and $\lambda_{DV} = 5.2 \times 10^{10}$ cm^3/g·day. All other parameter values are the same as in Tables 2 and 3.

https://doi.org/10.1371/journal.pone.0192449.g007

adequately represent the PDE model. For example, Fig 6 show antagonism between the OV and anti-PD-1, whereas this antagonism disappears in the ODE model.

Conclusion

Oncolytic virus (OV) is a genetically modified virus that can selectively invade cancer cells and replicate inside them. When an infected cell dies, its virus particles are released and proceed to infect other cancer cells. OV therapy, as a single agent, had not been successful because macrophages recognize infected cells and kill them together with their viruses. Recent studies use new designs of OV that can stimulate cytotoxic T cells to kill cancer cells before the viral population is significantly depleted by the macrophages. Some of these studies introduce enhancement of the T cells by blocking their checkpoints. Mice experiments demonstrated that both CTLA-4 and PD-L1 checkpoints blockade enhance the OV treatment [29–33]. There are recent clinical trials with OV and checkpoint inhibitors [34–37]. In particular, in clinical trials for melanoma, reported in [36], patients were treated with OV (T-VEC) and anti-CTLA-4 (ipilimumab) for a period of 13 weeks and were observed for an average period of 20 months.

Since T cells kill not only virus-free cancer cells but also virus-infected cancer cells, they may disrupt the anti-cancer effect of the OV. Hence an increase in the dose of the checkpoint inhibitor may actually have a pro-cancer effect. In order to clarify this situation we developed a mathematical model that includes the immune cells (macrophages, dendritic cells, and effective T cells), and characterized the OV by two parameters: the replication potential (λ_{V_i}) and its immunogenicity potential (λ_{DV}). We first simulated a treatment corresponding to mice experiments, where the dose γ_A of anti-PD-1 and the dose γ_V of OV were administered for 11 days, and the tumor volume was observed for 30 days. We found quantitative agreement with experimental results [49].

We then proceeded to use the model to run in *silico* clinical trials, where the treatment with a combination (γ_V, γ_A) was given for 14 weeks, and we observed the results of the treatment for 24 weeks. We simulated the tumor volume $V_{24}(\gamma_V, \gamma_A)$ at the end of 24 weeks for a range of (γ_V, γ_A). We found that there are regions in the (γ_V, γ_A)-plane where an increase in γ_A results in an increase in the tumor volume. Thus, there are regions of antagonism between the two drugs, where an increase in the anti-PD-1 decreases the efficacy of the treatment. We also simulated V_{24} (λ_{V_i}, γ_A) for a fixed parameter γ_V and variable (λ_{V_i}, γ_A). We again found regions of antagonism where an increase in γ_A results in an increase in the tumor volume.

These results have implications for clinical trials. Indeed for a clinical trial to be successful, the regions of antagonism between the doses of the checkpoint inhibitor and the OV doses should be determined early on, and avoided; these regions may depend on the specific oncolytic virus which is used in the clinical trial.

Materials and methods

Parameter estimation

Many of parameters in Tables 2 and 3 were taken directly from [38, 39, 50, 51]. When a value taken from these references was not obtained directly from experimental papers or was not carefully estimated from experimental results, we added an asterisk "*" next to the reference. These parameters were used in sensitivity analysis (see Figs 8 and 9) in order to see how the tumor value is affected by a random increase or decrease of these parameters by a factor of 2;

Table 2. Summary of parameter values.

Notation	Description	Value used	References
δ_D	diffusion coefficient of DCs	8.64×10^{-7} cm^2 day^{-1}	[38]*
δ_{T_1}	diffusion coefficient of CD4$^+$ T cells	8.64×10^{-7} cm^2 day^{-1}	[38]*
δ_{T_8}	diffusion coefficient of CD8$^+$ T cells	8.64×10^{-7} cm^2 day^{-1}	[38]*
δ_C	diffusion coefficient of tumor cells	8.64×10^{-7} cm^2 day^{-1}	[38]*
δ_M	diffusion coefficient of macrophages	8.64×10^{-7} cm^2 day^{-1}	[38]*
$\delta_{I_{12}}$	diffusion coefficient of IL-12	6.0472×10^{-2} cm^2 day^{-1}	[39]
δ_{I_2}	diffusion coefficient of IL-2	9.9956×10^{-2} cm^2 day^{-1}	[39]
δ_A	diffusion coefficient of IL-2	4.73×10^{-2} cm^2 day^{-1}	[39]
α_T	flux rate of T cells on the boundary	1 cm^{-1}	estimated
λ_C	growth rate of cancer cells	0.65 day^{-1}	estimated
λ_{V_i}	growth rate of intracellular virus	6×10^{-4} day^{-1}	estimated
λ_M	growth rate of macrophages	0.009 day^{-1}	[51]*
λ_{MC_i}	activation rate of macrophages by C_i	0.04 cm^3/g	estimated
λ_{DV}	activation rate of DCs by virus infection	5.2×10^{10} cm^3/g · day	estimated
λ_{DC}	activation rate of DCs by tumor cells	5.2 day^{-1}	estimated
$\lambda_{T_1 I_{12}}$	activation rate of CD4$^+$ T cells by IL-12	9.32 day^{-1}	[39]
$\lambda_{T_1 I_2}$	activation rate of CD4$^+$ T cells by IL-2	0.25 day^{-1}	[39]
$\lambda_{T_8 I_{12}}$	activation rate of CD8$^+$ T cells by IL-12	8.30 day^{-1}	[39]
$\lambda_{T_8 I_2}$	activation rate of CD8$^+$ T cells by IL-2	0.25 day^{-1}	[39]
$\lambda_{I_{12} D}$	production rate of IL-12 by DCs	2.76×10^{-6} day^{-1}	[39]
$\lambda_{I_2 T_1}$	production rate of IL-2 by CD4$^+$ T cells	2.82×10^{-8} day^{-1}	[39]
β_C	infection rate of cancer cells by virus	9×10^4 cm^3/g · day	estimated
β_V	rate of transition from V_e to V_i by infection	0.09 cm^3/g · day	estimated
$\mu_{C_i M}$	killing rate of C_i by M	4.8×10^{-2} cm^3/g · day	estimated
$\mu_{V_e M}$	clearance rate of V_e by M	2 cm^3/g · day	estimated
μ_{V_i}	death rate of infected cell due to viral burden	5×10^7 day^{-1}	estimated
N	burst size of V_i from natural death of C_i	100	estimated
η_8	killing rate of tumor cells by CD8$^+$ T cells	1.38×10^2 day^{-1} · cm^3/g	estimated
η_{8C_i}	killing rate of infected cancer cells by CD8$^+$ T cells	7.59×10^3 day^{-1} · cm^3/g	estimated
μ_{PA}	blocking rate of PD-1 by anti-PD-1	6.87×10^4 cm^3/g · day	[39]
ρ_P	expression of PD-1 in T cells	2.49×10^{-7}	[39]
ρ_L	expression of PD-L1 in T cells	5.22×10^{-7}	[39]
ε	relative expression of PD-L1 in tumor cells	0.01	[39]
d_C	death rate of uninfected tumor cells	0.17 day^{-1}	[50]*
d_M	death rate of macrophages	0.015 day^{-1}	[51]
d_D	death rate of DCs	0.1 day^{-1}	[50]
d_{T_1}	death rate of CD4$^+$ T cells	0.197 day^{-1}	[50]
d_{T_8}	death rate of CD8$^+$ T cells	0.18 day^{-1}	[50]
$d_{I_{12}}$	degradation rate of IL-12	1.38 day^{-1}	[50]
d_{I_2}	degradation rate of IL-2	2.376 day^{-1}	[50]

* In this reference the value was estimated but not obtained directly from experimental results.

https://doi.org/10.1371/journal.pone.0192449.t002

Table 3. Summary of parameter values.

K_C	half-saturation of tumor cells	0.4 g/cm^3	[50]
K_D	half-saturation of DCs	0.4×10^{-4} g/cm^3	[39]
$K_{I_{12}}$	half-saturation of IL-12	1.5×10^{-10} g/cm^3	[50]
K_{I_2}	half-saturation of IL-2	2.37×10^{-11} g/cm^3	[50]
K_{T_1}	half-saturation of CD4$^+$ T cells	2×10^{-3} g/cm^3	[39]
K_{T_8}	half-saturation of CD8$^+$ T cells	1×10^{-3} g/cm^3	[39]
K'_{TQ}	inhibition of function of T cells by PD-1-PD-L1	1.365×10^{-18} g/cm^3	[39]*
θ	total cell density	0.6034 g/cm^3	**
D_0	density of immature DCs	2×10^{-5} g/cm^3	[50]
T_{10}	density of naive CD4$^+$ T cells	4×10^{-4} g/cm^3	[39]*
T_{80}	density of naive CD8$^+$ T cells	2×10^{-4} g/cm^3	[39]*
C_M	carrying capacity of cancer cells	0.8 g/cm^3	[50]
$\hat{T}_1$	density of CD4$^+$ T cells from lymph node	4×10^{-3} g/cm^3	[39]*
$\hat{T}_8$	density of CD8$^+$ T cells from lymph node	2×10^{-3} g/cm^3	[39]*

* In this reference the value was estimated but not obtained directly from experimental results.

** The value is determined by Eq (1) with steady state densities of the cells.

https://doi.org/10.1371/journal.pone.0192449.t003

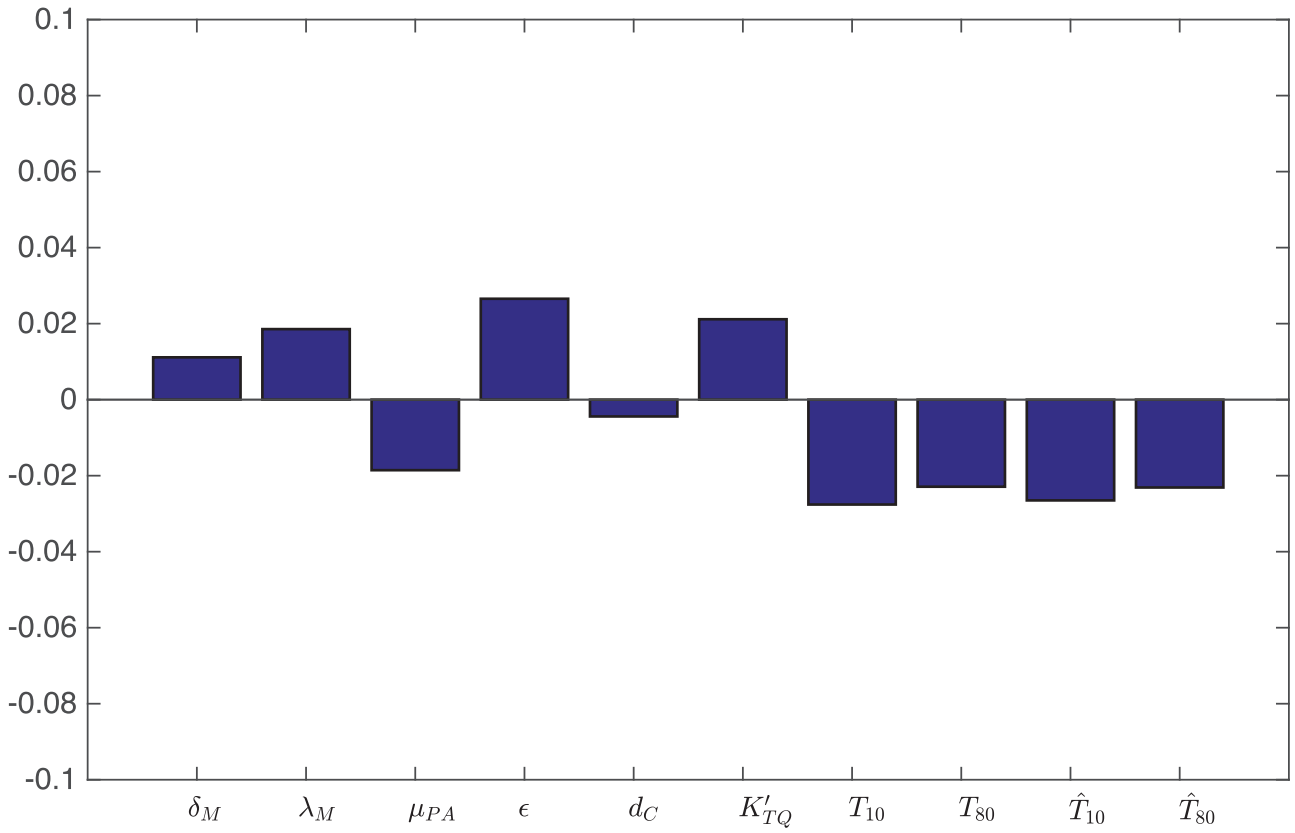

Fig 8. Statistically significant PRCC values (p-value$<$ 0.01) for $R(t)$ at day 60.

https://doi.org/10.1371/journal.pone.0192449.g008

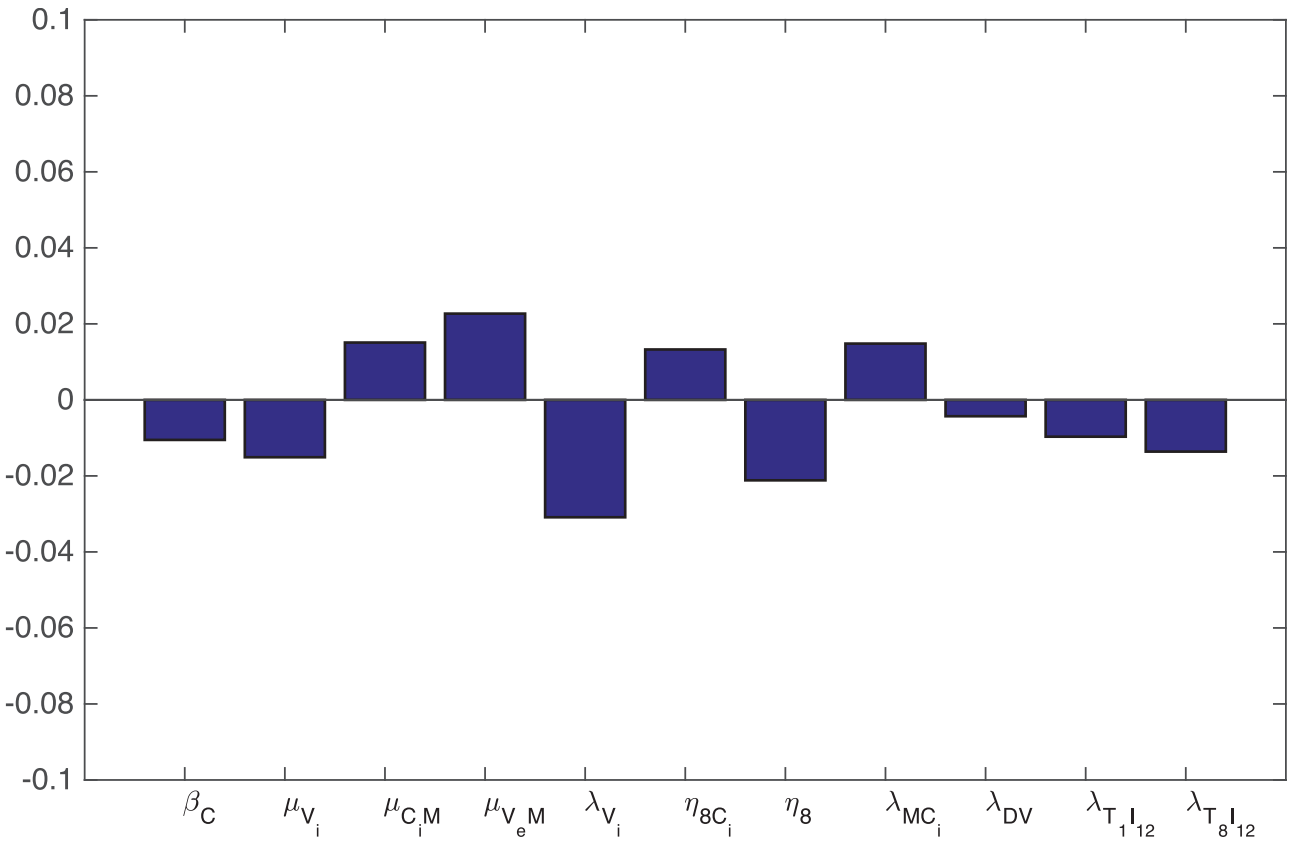

Fig 9. Statistically significant PRCC values (p-value$<$ 0.01) for $R(t)$ at day 60.

https://doi.org/10.1371/journal.pone.0192449.g009

but the dispersion coefficient of macrophages was increased by up to a factor of 4 because they are highly mobile.

Diffusion coefficients. The diffusion coefficients of cytokines were computed in [39] based on the formula

$$\delta_p = \frac{A}{M_p^{1/3}},$$

where A is a constant and p is any protein with diffusion coefficient δ_p and molecular weight M_p. The diffusion coefficients of cells may vary depending on the cell type. For simplicity we take them equal, and choose the common value as in [39], but we show in the section on sensitivity analysis that the tumor growth is affected very little by taking different diffusion coefficients for different cell types.

Half-saturation. In an expression of the form $Y\frac{X}{K_X+X}$ where Y is activated by X, the parameter K_X is called the *half-saturation* of X. If X reaches a steady state X_0, we expect that $X_0/(K_X + X_0)$ will not be "too close" to 0 and not "too close" to 1. For definiteness we take $X_0/(K_X + X_0)$ to be 1/2, so that

$$K_X = X_0;$$

the steady state X_0 is derived from experimental or clinical data.

Eq (2). We take $\lambda_C = 0.65$/day, which is slightly smaller than in [38], and $\beta_C = 9 \times 10^4$ cm^3/g · day, which is slightly larger than in [52], and we take $\eta_8 = 1.38 \times 10^2$ cm^3/g · day, which is slightly larger than in [39].

Eq (3). We assume that T_8 cells kill C_i much more efficiently than they kill C, and take $\eta_{8C_i} = 55\eta_8 = 7.59 \times 10^3$ cm^3/g · day. We assume that OV is designed to stimulate the immune system while it is in infected cells. Therefore the viral burden does not increase the death rate of infected cells very much. We therefore take $\mu_{V_i} = 2 \times 10^7$ cm^3/g so that $\mu_{V_i} V_i$ is very small compared to 1, e.g. it increases the death of the infected cancer cell by 2% when the viral load is 10^{-9} g/cm^3. Macrophages engulf infected cancer cells [40], but we assume that the rate is extremely small compared to the rate by which T_8 kill infected cancer cells. We accordingly take $\mu_{C_i M} = 4.8 \times 10^{-2}$/day.

Eqs (4) and (5). We take $N = 100$, which is in the range considered in [51]. We assume that the ratio of mass of one virus to one cell is $m_{VC} = 10^{-6}$. Hence $\beta_V = \beta_C m_{VC} = 0.09$ cm^3/g · day. We assume that the clearance rate of V_e by macrophages is much larger than the rate by which V_e invades uninfected cancer cells, and take $\mu_{V_e M} = 2$ cm^3/g · day. We assume that the ratio of C_i/V_i in the first 12 days averages 3×10^6, and that the replication of an intracellular virus occurs approximately every 22-23 hours, so that the growth rate per day is $1.5 \times 2^9 V_i$. Hence $\lambda_{V_i} C_i = \lambda_{V_i}\left(\frac{C_i}{V_i}\right) V_i = \left(\lambda_{V_i} \times 3 \times 10^6\right) V_i$ and the growth rate of V_i is then determined by the equation $(\lambda_{V_i} \times 3 \times 10^6) V_i = 1.5 \times 2^9 V_i$, so that $\lambda_{V_i} = 6 \times 10^{-4}$/day.

Eq (6). Without OV, we assume $\lambda_M = d_M M$ in steady state, where $d_M = 0.015$/day and $M = K_M = 0.2$ g/cm^3. Hence $\lambda_M = 0.003$/day. We note however that in estimating λ_M, we ignored the contribution of $\nabla \cdot (\mathbf{u}M)$, whose integral over the tumor $\{r < R(t)\}$ is $\int_{r=R(t)} \frac{dR(t)}{dt} \cdot M$, which is a positive quantity. Hence, $\frac{\partial M}{\partial t}$ is actually decreased when we equate to zero the right-hand side (RHS) of Eq (6); we therefore need to increase λ_M; we take $\lambda_M = 0.09$/day. Since initially tumor is with radius $R(0) = 0.01$ cm, macrophages had already arrived into the tumor tissue so that the additional increase in macrophages, $\lambda_{MC_i} MC_i$, is assumed to be 'relatively' small; we take $\lambda_{MC_i} = 0.04$ cm^3/g.

Eq (7). We take $\lambda_{DC} = 5.2$/day which is slightly larger than in [39]. We assume that the virus, although having decreased over time, is still effective in activating dendritic cells, so that $\lambda_{DV} V_i$ is comparable to λ_{DC} when $V_i \approx 10^{-10}$ g/cm^3. Accordingly, we take $\lambda_{DV} = 5.2 \times 10^{10}$ cm^3/g · day.

Sensitivity analysis

We performed sensitivity analysis with respect to the tumor volume at day 30 for two sets of parameters. The first set consists of parameters marked by "*" in Tables 2 and 3. These parameters were not derived, or not carefully estimated, from experimental or clinical data. These parameters are: δ_C, δ_M, δ_D, δ_{T_1}, δ_{T_8}, λ_M, μ_{PA}, ε, d_C, K'_{TQ}, T_{10}, T_{80}, $\hat{T}_1$, $\hat{T}_8$. Following the method of [53], we performed Latin hypercube sampling and generated 5000 samples to calculate the partial rank correlation coefficients (PRCC) and the p-values with respect to the tumor volume at day 30. In sampling all the parameters, we took the range of each parameter (except the diffusion coefficients) from 1/2 to twice its value in Tables 2 or 3. In the simulations of the model we assumed that the diffusion coefficients of all the cell types are equal. What may cause a significant difference in the simulations is actually the differences between the diffusion coefficients of cell types, rather than their actual values. Since macrophages are highly mobile, we chose to include only δ_M in the sensitivity analysis, keeping all other diffusion coefficient equal, and randomly increasing δ_M by up to a factor of 4. The results are shown in Fig 8. We

see that increasing the source of T cells (T_{10}, T_{80}, $\hat{T}_{10}$, $\hat{T}_{80}$) decreases the tumor volume, as does the depletion rate (μ_{PA}) of PD-1 by the PD-1 inhibitor. On the other hand the production rate of PD-L1 by the cancer (ε) increases the tumor volume. An increase of the random mobility of macrophages, by a factor up to 4, only slightly increases the tumor volume.

The second set of parameters in the sensitivity analysis are some production parameters, namely λ_{V_i}, λ_{MC_i}, λ_{DV}, $\lambda_{T_1I_{12}}$ and $\lambda_{T_8I_{12}}$, and the parameters β_C, μ_{V_i}, $\mu_{C_i M}$, η_8, η_{8C_i} and d_{V_eM} which play important roles in the dynamics of C. Here again we sampled all the parameters by taking the range of each parameter for 1/2 to twice its value in Tables 2 and 3. The results are shown in Fig 9.

It is interesting to see from Fig 9 that the parameters that promote killing of infected cancer cells, such as μ_{C_iM}, μ_{V_eM}, η_{8C_i} and λ_{MC_i} are positively correlated with the tumor volume, while the parameters that promote viral infection, such as β_C, μ_{V_i} and λ_{V_i}, are negatively correlated with the tumor volume. We also see that the production/activation rates that promote effector T cells, namely, λ_{DV}, $\lambda_{T_1I_{12}}$ and $\lambda_{T_8I_{12}}$, are negatively correlated to the tumor volume, while the killing rate of uninfected cancer cells cells by $CD8^+$ T cells, η_8, is negatively correlated with tumor volume.

Computational method

We employ moving mesh method [48] to numerically solve the free boundary problem for the tumor proliferation model. To illustrate this method, we take Eq (2) as example and rewrite it as the following form:

$$\frac{\partial C(r,t)}{\partial t} = \delta_C \Delta C(r,t) - div(\mathbf{u}C) + F, \tag{22}$$

where F represents the term in the right hand side of Eq (2). Let r_i^k and C_i^k denote numerical approximations of i-th grid point and $C(r_i^k, n\tau)$, respectively, where τ is the size of time-step. The discretization of Eq (22) is derived by the fully implicit finite difference scheme:

$$\frac{C_i^{k+1} - C_i^k}{\tau} = \delta_C \left(C_{rr} + \frac{2}{r_i^k} C_r \right) - \left(\frac{2}{r_i^{k+1}} u_i^{k+1} + u_r \right) C_i^{k+1} - u_i^{k+1} C_r + F_i^{k+1}, \tag{23}$$

where $C_r = \frac{h_{-1}^2 C_{i+1}^{k+1} - h_1^2 C_{i-1}^{k+1} - (h_1^2 - h_{-1}^2) C_i^{k+1}}{h_1 (h_{-1}^2 - h_1 h_{-1})}$, $C_{rr} = 2 \frac{h_{-1} C_{i+1}^{k+1} - h_1 C_{i-1}^{k+1} + (h_1 - h_{-1}) C_i^{k+1}}{h_1 (h_1 h_{-1} - h_{-1}^2)}$,

$u_r = \frac{h_{-1}^2 u_{i+1}^{k+1} - h_1^2 u_{i-1}^{k+1} - (h_1^2 - h_{-1}^2) u_i^{k+1}}{h_1 (h_{-1}^2 - h_1 h_{-1})}$, $h_{-1} = r_{i-1}^{k+1} - r_i^{k+1}$ and $h_1 = r_{i+1}^{k+1} - r_i^{k+1}$. The mesh moves by $r_i^{k+1} = r_i^k + u_i^{k+1}\tau$, where u_i^{k+1} is solved by the velocity equation.

Acknowledgments

This work is supported by the Mathematical Biosciences Institute and the National Science Foundation (Grant DMS 0931642), and by the Renmin University of China and the International Postdoctoral Exchange Fellowship Program 2016 by the Office of China Postdoctoral Council.

Author Contributions

Conceptualization: Avner Friedman, Xiulan Lai.

Data curation: Avner Friedman, Xiulan Lai.

Formal analysis: Avner Friedman, Xiulan Lai.

Funding acquisition: Avner Friedman, Xiulan Lai.

Investigation: Avner Friedman, Xiulan Lai.

Methodology: Avner Friedman, Xiulan Lai.

Project administration: Avner Friedman, Xiulan Lai.

Resources: Avner Friedman, Xiulan Lai.

Software: Avner Friedman, Xiulan Lai.

Supervision: Avner Friedman, Xiulan Lai.

Validation: Avner Friedman, Xiulan Lai.

Visualization: Avner Friedman, Xiulan Lai.

Writing – original draft: Avner Friedman, Xiulan Lai.

Writing – review & editing: Avner Friedman, Xiulan Lai.

References

1. Cheng, X, Veverka, V, Radhakrishnan, A, Waters, LC, Muskett, FW, Morgan, SH, et al. Human PD-L1/B7-H1/CD274 Protein. Sino Biological Inc, http://wwwsinobiologicalcom/PD-L1-B7-H1-CD274-Protein-g-533html;.
2. Shi L, Chen S, Yang L, Li Y. The role of PD-1 and PD-L1 in T-cell immune suppression in patients with hematological malignancies. J Hematol Oncol. Sep 2013; 6(74).
3. Muppidi MR, George S. Immune Checkpoint Inhibitors in Renal Cell Carcinoma. Journal of Targeted Therapies in Cancer 2015. 2015; 4:47–52.
4. Buchbinder EI, Desai A. CTLA-4 and PD-1 Pathways: Similarities, Differences, and Implications of Their Inhibition. Am J Clin Oncol. February 2016; 39(1):98–106. https://doi.org/10.1097/COC.0000000000000239 PMID: 26558876
5. Postow MA, Callahan MK, Wolchok JD. Immune Checkpoint Blockade in Cancer Therapy. Journal of Clinical Oncology. June 2015; 33(17):1974–1982. https://doi.org/10.1200/JCO.2014.59.4358 PMID: 25605845
6. He J, Hu Y, Hu M, Li B. Development of PD-1/PD-L1 Pathway in Tumor Immune Microenvironment and Treatment for Non-Small Cell Lung Cancer. Scientific Reports. Aug 2015; 5(13110).
7. Blank CU, Enk A. Therapeutic use of anti-CTLA-4 antibodies. Int Immunol. Janurary 2015; 27(1):3–10. https://doi.org/10.1093/intimm/dxu076 PMID: 25038057
8. Funt SA, Page DB, Wolchok JD, Postow MA. CTLA-4 antibodies: new directions, new combinations. Oncology (Williston Park). November 2014; Suppl 3:6–14.
9. Heo J, Reid T, Ruo L, Breitbach CJ, Rose S, Bloomston M, et al. Randomized dose-finding clinical trial of oncolytic immunotherapeutic vaccinia JX-594 in liver cancer. Nat Med. February 2013; 19(3):329–336. https://doi.org/10.1038/nm.3089 PMID: 23396206
10. Hwang TH, Moon A, Burke J, Ribas A, Stephenson J, Breitbach CJ, et al. A mechanistic proof-of-concept clinical trial with JX-594, a targeted multi-mechanistic oncolytic poxvirus, in patients with metastatic melanoma. Mol Ther. October 2011; 19(10):1913–1922. https://doi.org/10.1038/mt.2011.132 PMID: 21772252
11. Markert JM, Liechty PG, Wang W, Gaston S, Braz E, Karrasch M, et al. Phase Ib trial of mutant herpes simplex virus G207 inoculated pre-and post-tumor resection for recurrent GBM. Mol Ther. January 2009; 17(1):199–207. https://doi.org/10.1038/mt.2008.228 PMID: 18957964
12. Nakao A, Kasuya H, Sahin TT, Nomura N, Kanzaki A, Misawa M, et al. A phase I dose-escalation clinical trial of intraoperative direct intratumoral injection of HF10 oncolytic virus in non-resectable patients with advanced pancreatic cancer. Cancer Gene Ther. 2009; 18(3):167–175. https://doi.org/10.1038/cgt.2010.65
13. Patel MR, Kratzke RA. Oncolytic virus therapy for cancer: the first wave of translational clinical trials. Transl Res. 2013; 161(4):355–364. https://doi.org/10.1016/j.trsl.2012.12.010 PMID: 23313629
14. Tönjes M, Barbus S, Park YJ, Wang W, Schlotter M, Lindroth AM, et al. BCAT1 promotes cell proliferation through amino acid catabolism in gliomas carrying wild-type IDH1. Nat Med. February 2013; 19(7):901–908. https://doi.org/10.1038/nm.3217 PMID: 23793099

15. Fulci G, Dmitrieva N, Gianni D, Fontana EJ, Pan X, Lu Y, et al. Depletion of peripheral macrophages and brain microglia increases brain tumor titers of oncolytic viruses. Cancer Res. 2007; 67(19):9398–9406. https://doi.org/10.1158/0008-5472.CAN-07-1063 PMID: 17909049

16. Thorne SH, Liang W, Sampath P, Schmidt T, Sikorski R, Beilhack A, et al. Targeting localized immune suppression within the tumor through repeat cycles of immune cell-oncolytic virus combination therapy. Mol Ther. 2010; 18(9):1698–1705. https://doi.org/10.1038/mt.2010.140 PMID: 20606649

17. Lun X, Yang W, Alain T, Shi ZQ, Muzik H, Barrett JW, et al. Myxoma virus is a novel oncolytic virus with significant antitumor activity against experimental human gliomas. Cancer Res. 2005; 65(21):9982–9990. https://doi.org/10.1158/0008-5472.CAN-05-1201 PMID: 16267023

18. Meisen WH, Wohleb ES, Jaime-Ramirez AC, Bolyard C, Yoo JY, Russell L, et al. The impact of macrophage and microglia secreted TNF alpha on oncolytic HSV-1 therapy in the glioblastoma tumor microenvironment. Clin Cancer Res. July 2015;(21):3274–3285. https://doi.org/10.1158/1078-0432.CCR-14-3118 PMID: 25829396

19. Özduman K, Wollmann G, Piepmeier JM, van den Pol AN. Systemic vesicular stomatitis virus selectively destroys multifocal glioma and metastatic carcinoma in brain. J Neurosci. 2008; 28(8):1882–1893. https://doi.org/10.1523/JNEUROSCI.4905-07.2008

20. Wollmann G, Rogulin V, Simon I, Rose JK, van den Pol AN. Some attenuated variants of vesicular stomatitis virus show enhanced oncolytic activity against human glioblastoma cells relative to normal brain cells. J Virol. February 2010; 84(3):1563–1573. https://doi.org/10.1128/JVI.02040-09 PMID: 19906910

21. Fournier P, Schirrmacher V. Oncolytic Newcastle Disease Virus as Cutting Edge between Tumor and Host. Biology (Basel). September 2013; 2(3):936–975.

22. Thorne SH, Hwang THH, O' Gorman WE, Bartlett DL, Sei S, Kanji F, et al. Rational strain selection and engineering creates a broad-spectrum, systemically effective oncolytic poxvirus, JX-963. J Clin Invest. 2007; 117(11):3350–3358. https://doi.org/10.1172/JCI32727 PMID: 17965776

23. Wang LCS, Lynn RC, Cheng G, Alexander E, Kapoor V, Moon EK, et al. Treating tumors with a vaccinia virus expressing IFNbeta illustrates the complex relationships between oncolytic ability and immunogenicity. Mol Ther. 2012; 20(4):736–748. https://doi.org/10.1038/mt.2011.228 PMID: 22008913

24. Aref S, Bailey K, Fielding A. Measles to the rescue: A review of oncolytic measles virus. Viruses. October 2016; 8(10):294. https://doi.org/10.3390/v8100294

25. Koks CAE, De Vleeschouwer S, Graf N, Van Gool SW. Immune suppression during oncolytic virotherapy for high-grade glioma; Yes or No? J Cancer. January 2015; 6(3):203–217. https://doi.org/10.7150/jca.10640 PMID: 25663937

26. Melzer MK, Lopez-Martinez A, Altomonte J. Oncolytic Vesicular Stomatitis Virus as a Viro-Immunotherapy: Defeating Cancer with a 'Hammer' and 'Anvil'. Biomedicines. February 2017; 5(1):8. https://doi.org/10.3390/biomedicines5010008

27. Hernández-Alcoceba R. Recent advances in oncolytic virus design. Clinical and Translational Oncology. 2011; 13(4):229–239. https://doi.org/10.1007/s12094-011-0647-4 PMID: 21493183

28. Maroun J, Muñoz-Alía M, Ammayappan A, Schulze A, Peng KW, Russell S. Designing and building oncolytic viruses. Future Virology. 2017; 12(4):193–213. https://doi.org/10.2217/fvl-2016-0129

29. Zamarin D, Holmgaard RB, Subudhi SK, Park JS, Mansour M, Palese P, et al. Localized oncolytic virotherapy overcomes systemic tumor resistance to immune checkpoint blockade immunotherapy. Sci Transl Med. March 2014; 6(226):226ra32. https://doi.org/10.1126/scitranslmed.3008095 PMID: 24598590

30. Engeland CE, Grossardt C, Veinalde R, Bossow S, Lutz D, Kaufmann JK, et al. CTLA-4 and PD-L1 checkpoint blockade enhances oncolytic measles virus therapy. Mol Ther. November 2014; 22(11):1949–1959. https://doi.org/10.1038/mt.2014.160 PMID: 25156126

31. Rojas JJ, Sampath P, Hou W, Thorne SH. Defining Effective Combinations of Immune Checkpoint Blockade and Oncolytic Virotherapy. Clin Cancer Res. December 2015; 21(24):5543–5551. https://doi.org/10.1158/1078-0432.CCR-14-2009 PMID: 26187615

32. Dias JD, Hemminki, Diaconu I, Hirvinen M, Bonetti A, Guse K, et al. Targeted cancer immunotherapy with oncolytic adenovirus coding for a fully human monoclonal antibody specific for CTLA-4. Gene Ther. November 2012; 19(10):988–998. https://doi.org/10.1038/gt.2011.176 PMID: 22071969

33. Rajani KR, Vile RG. Harnessing the Power of Onco-Immunotherapy with Checkpoint Inhibitors. Viruses. November 2015; 7(11):5889–5901. https://doi.org/10.3390/v7112914 PMID: 26580645

34. Johnson DB, Puzanov I, Kelley MC. Talimogene laherparepvec (T-VEC) for the treatment of advanced melanoma. Immunotherapy. 2015; 7(6):611–619. https://doi.org/10.2217/imt.15.35 PMID: 26098919

35. Fonteneau J. Oncolytic Viruses and Immune Checkpoint Inhibitors. Immunother Open Acc. 2016; 2(e105).

36. Puzanov I, Milhem MM, Minor D, Hamid O, Li A, Chen L, et al. Talimogene laherparepvec in combination with ipilimumab in previously untreated, unresectable stage IIIB-IV melanoma. Journal of Clinical Oncology. 2016; 34(22):2619–2626. https://doi.org/10.1200/JCO.2016.67.1529 PMID: 27298410

37. Dummer R, Hoeller C, Gruter IP, Michielin O. Combining talimogene laherparepvec with immunotherapies in melanoma and other solid tumors. Cancer Immunol, Immunother. 2017; 66(6):683–695. https://doi.org/10.1007/s00262-017-1967-1

38. Lai X, Friedman A. Combination therapy of cancer with cancer vaccine and immune checkpoint inhibitor: A mathematical model. PLoS ONE. 2017; 12(2):e0178479. https://doi.org/10.1371/journal.pone.0178479 PMID: 28542574

39. Lai X, Friedman A. Combination therapy of cancer with BRAF inhibitor and immune checkpoint inhibitor: A mathematical model. BMC System Biology. 2017; 11(70).

40. Feng M, Chen JY, Weissman-Tsukamoto R, Volkmer JP, Ho PY, McKenna KM, et al. Macrophages eat cancer cells using their own calreticulin as a guide: roles of TLR and Btk. Proceedings of the National Academy of Sciences. 2015; 112(7):2145–2150. https://doi.org/10.1073/pnas.1424907112

41. Palucka J, Banchereau J. Cancer immunotherapy via dendritic cells. Nat Rev Cancer. Mar 2012; 12 (4):265–277. https://doi.org/10.1038/nrc3258 PMID: 22437871

42. Saenz R, Futalan D, Leutenez L, Eekhout F, Fecteau JF, Sundelius S, et al. TLR4-dependent activation of dendritic cells by an HMGB1-derived peptide adjuvant. J Transl Med. Aug 2014; 12(211):1–11.

43. Sims GP, Rowe DC, Rietdijk ST, Herbst R, Coyle AJ. HMGB1 and RAGE in inflammation and cancer. Annu Rev Immunol. 2010; 28:367–388. https://doi.org/10.1146/annurev.immunol.021908.132603 PMID: 20192808

44. Janco JMT, Lamichhane P, Karyampudi L, Knutson KL. Tumor-infiltrating dendritic cells in cancer pathogenesis. J Immunol. Apr 2015; 194(7):2985–2991. https://doi.org/10.4049/jimmunol.1403134

45. Ma Y, Shurin GV, Peiyuan Z, Shurin MR. Dendritic Cells in the Cancer Microenvironment. J Cancer. 2013; 4(1):36–44. https://doi.org/10.7150/jca.5046 PMID: 23386903

46. Cheng X, Veverka V, Radhakrishnan A, Waters LC, Muskett FW, Morgan SH, et al. Structure and interactions of the human programmed cell death 1 receptor. J Biol Chem. Apr 2013; 288(17):11771–11785. https://doi.org/10.1074/jbc.M112.448126 PMID: 23417675

47. Mautea RL, Gordona SR, Mayere AT, McCrackena MN, Natarajane A, Ring NG, et al. Engineering high-affinity PD-1 variants for optimized immunotherapy and immuno-PET imaging. Proc Natl Acad Sci USA. Nov 2015; 112(47):E6506–14. https://doi.org/10.1073/pnas.1519623112

48. D'Acunto B. Computational Methods for PDE in mechanics. Series on Advances in Mathematics for Applied Sciences-Vol.67. Singapore: Word Scientific; 2004.

49. Chen CY, Wang PY, Hutzen B, Sprague L, Swain HM, Love JK, et al. Cooperation of oncolytic Herpes virotherapy and PD-1 blockade in murine Rhabdomyosarcoma models. Scientific Reports. May 2017; 7 (2396):1–10.

50. Hao W, Friedman A. The role of exosomes in pancreatic cancer microenvironment. Bull Math Biol. April 2017;

51. Jacobsen K, Russell L, Kaur B, Friedman A. Effects of CCN1 and Macrophage Content on Glioma Virotherapy: A Mathematical Model. Bull Math Biol. June 2015; 77(6):984–1012. https://doi.org/10.1007/s11538-015-0074-8 PMID: 25758754

52. Ratajczyk E, Ledzewicz U, Leszczynski M, Friedman A. The role of TNF-alpha inhibitor in glioma virotherapy: A mathematical model. Math Biosci Eng. February 2017; 1(14):305–319.

53. Marino S, Hogue I, Ray C, Kirschner D. A methodology for performing global uncertainty and sensitivity analysis in systems biology. J Theor Biol. 2008; 254(1):178–196. https://doi.org/10.1016/j.jtbi.2008.04.011 PMID: 18572196